

CONDITION MONITORING OF A WIND TURBINE DFIG BY CURRENT OR POWER ANALYSIS

*C.J. Crabtree**, *S. Djurović[†]*, *P.J. Tavner**, *A.C. Smith[†]*

** School of Engineering and Computing Sciences, Durham University, UK, c.j.crabtree@durham.ac.uk*

[†] School of Electrical and Electronic Engineering, University of Manchester, UK, sinisa.durovic@manchester.ac.uk

Keywords: wind turbine, condition monitoring, power, current.

Abstract

As wind energy assumes greater importance in remote and offshore locations, effective and reliable condition monitoring techniques are required. This paper proposes a method analysing electrical signals from the stator terminals of the wound rotor induction generators commonly used in wind turbines. Analytical equations have been derived for the frequency content of line current and total instantaneous power for healthy and faulty wound rotor induction generators and these have been used to analyse signals from test rigs in the steady state. Analysis at constant speed yields a set of equation constants which describe the frequencies of most interest as observed from the test rig environments. Having discovered a consistent group of fault frequencies the data is then demonstrated at variable speed to show the variability of those fault frequencies with speed. It is concluded that tracking these speed dependent fault frequencies will be an effective way to monitor the health of a wound rotor induction generator in a wind turbine.

1 Introduction

As wind turbines (WT) increase in capacity and move to less accessible, offshore environments condition monitoring of WTs and their electrical generators will become essential to reduce downtime and improve capacity factors. The Doubly Fed Induction Generator (DFIG) is one of the favoured conversion devices for WTs with rating in excess of 1MW [1]. Prompt fault detection in these machines is essential to enable timely maintenance for incipient generator faults, which otherwise may have a catastrophic effect on the WT drive train and system operation. Reliable and effective condition monitoring is therefore gaining greater importance and generator defects have been shown to be a major contributor to WT downtime.

This work investigates the effect of unbalanced rotor windings on the generator stator current and total instantaneous power signals, firstly under steady state, constant speed test operation and secondly under transient, variable speed conditions such as encountered in a WT. Both current and power frequency domain analysis are commonly used in algorithms for fault detection in cage rotor induction

machines [5][2] and power signal analysis has been demonstrated for fault detection on an operational WT [4]. This work evaluates their potential to provide reliable indications of rotor unbalance for a wound rotor induction generator (WRIG) like the DFIGs used in WTs. The analysis described is based on experimental data obtained from two different WRIG test rigs, one at Durham University and the other at the University of Manchester.

This paper first discusses analytical expressions for the origins of stator harmonic content as given in [6] before using steady state experimental data to further enhance the theory. Based on results in the steady state conclusions will be drawn about frequencies of interest for condition monitoring. Finally an example of tracking specific fault-related frequencies in a variable speed test rig, like a WT, will be presented and discussed as a medium for condition monitoring.

2 Analytical and Experimental Tools

2.1 Analytical Expressions

Previous work at the University of Manchester [6] provides the analytical expressions necessary to calculate the harmonic content of the current and power signals of a WRIG. In this work we consider the effect of rotor winding or brush gear unbalance and so only the equations relating to this particular type of asymmetry are presented. However, previous work [3] includes further expressions for various machine electrical faults. Equations (1) and (2) give all possible frequencies in the healthy and faulty WRIG current signals respectively. Not all of these harmonic frequencies will be clear for all machines as they will be attenuated or highlighted by various machine design artefacts or operating conditions.

$$f_{ind}^k = |6k(1-s) \pm l|f \quad (1)$$

$$f_{ind}^k = \left| \frac{k}{p}(1-s) \pm l \right| f \quad (2)$$

where f is the fundamental supply frequency, s is the WRIG slip, $k = 0,1,2,\dots$ and $l = 1,2,3,\dots$. Constants k and l relate respectively to air-gap field space harmonics resulting from the layout of the machines and supply time harmonics in the current.

These expressions can also be given for the total instantaneous power signal of a WRIG. Equations (3) and (4) give all possible harmonic components in the total power signal for healthy and faulty machines, respectively.

$$f_{ind}^k = |j \pm 6k(1-s) \pm l|f \quad (3)$$

$$f_{ind}^k = \left| j \pm \frac{k}{p}(1-s) \pm l \right| f \quad (4)$$

where $j = 1, 2, 3, \dots$, $k = 0, 1, 2, \dots$ and $l = 1, 2, 3, \dots$. The additional constant j relates to supply time harmonics in the voltage. A detailed derivation of these expressions will be provided in a separate paper.

2.2 Experimental Test Rigs

Having obtained analytical expressions for all possible frequencies in both the line current and total instantaneous power tests were carried out to confirm these against experimental data. Two test rigs have been used for this, at the Universities of Manchester and Durham.

The Manchester test rig comprises a 4-pole, three phase 30kW WRIG mechanically coupled to a 40kW DC motor by a common shaft. The DC motor speed is regulated by means of an industrial variable speed drive allowing a range of operating points to be achieved. The WRIG rotor windings are short circuited and the stator windings are connected to the grid via a three phase Variac. For the purpose of these tests the WRIG was run up to the required super-synchronous speed and the stator voltage gradually increased until the

required value was realised. Current and voltage probes were installed in the WRIG stator circuit for measurement purposes and these sampled simultaneously using a precision digital oscilloscope. To reduce noise in the total instantaneous power signal the two wattmeter method was used for its calculation.

Similarly, the Durham test rig features a 4-pole, 30kW WRIG of identical manufacture and altered winding arrangements but driven through a 5:1 two stage gearbox by a 54kW DC motor. A variable speed drive allowed the test rig to achieve similar steady state operating points as used at Manchester. Again, two phase voltages and line currents were sampled by the same set of current and voltage probes and a precision oscilloscope to ensure consistency between results for steady state operation. Further to this, the Durham test rig can be driven using shaft speed data from a detailed wind turbine model, allowing realistic variable speed operation. The test rig and driving conditions have been previously discussed in [7]. Data acquisition in this case was carried out using a National Instruments data acquisition system and the three-wattmeter method to calculate the total power signal. An accurate speed signal was also recorded for use in a frequency tracking algorithm. In order to allow for variable speed driving using the 54kW DC motor a small amount of additional resistance was added in the WRIG rotor circuit allowing a WRIG speed variation of 100rev/min (7% slip) above synchronous. The rotor phase resistance for the healthy WRIG was 1.2Ω .

For the Manchester WRIG with a 'healthy' rotor the shorted rotor phase resistance was 0.06Ω . In order to emulate a brush gear or winding fault an additional resistance of 0.3Ω was introduced into one phase of the star-connected rotor. In order

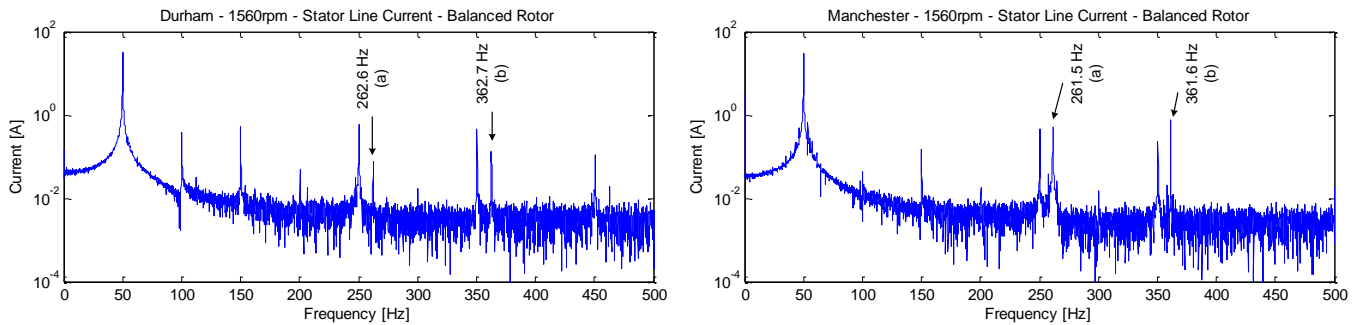


Figure 1: Line current spectra for the healthy test rigs at 1560rpm

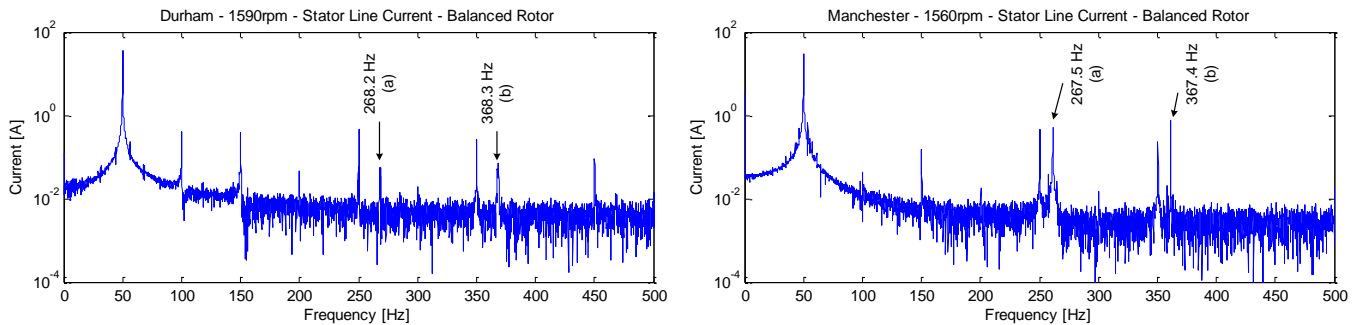


Figure 2: Line current spectra for the healthy test rigs at 1590rpm

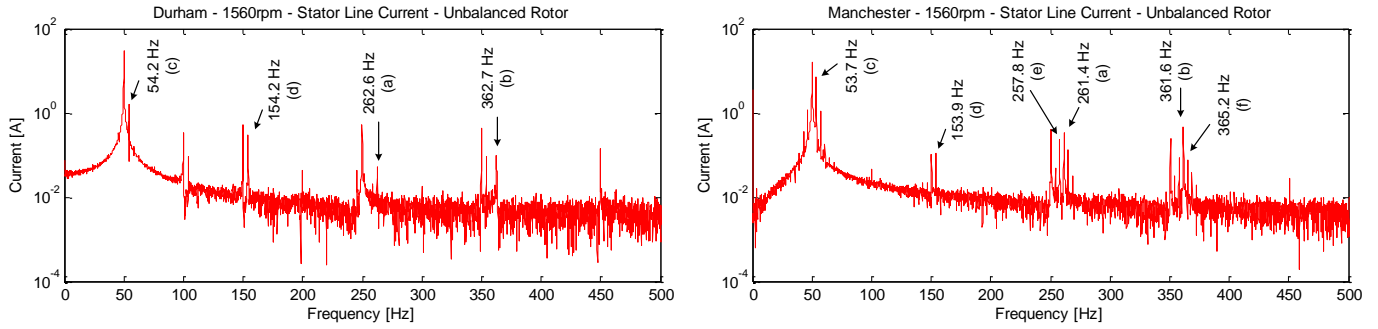


Figure 3: Line current spectra for the faulty test rigs at 1560rpm

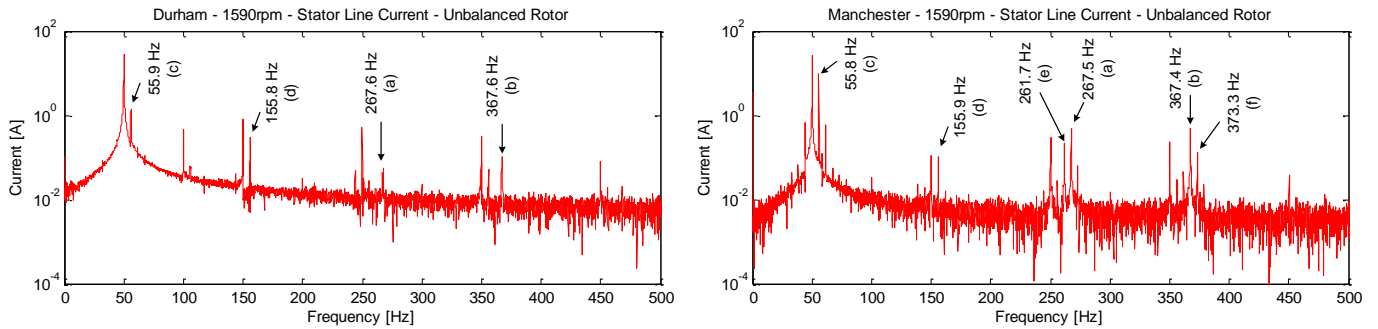


Figure 4: Line current spectra for the faulty test rigs at 1590rpm

to achieve the same speed range at Durham the ‘healthy’ phase resistance was increased to 1.2Ω per phase with an additional resistance of 1.2Ω added in one phase for the unbalanced condition. This change in resistance is not unreasonable for a machine with brush gear damage.

3 Results in the Steady State

3.1 Line Current Results

In order to practically verify the results of equations (1) to (4) a series of tests were carried out using both test rigs. Three arbitrary speed points, achievable on both test rigs were selected for comparison. The test rigs were run at constant, super-synchronous speeds of 1530, 1560 and 1590 rev/min under both healthy and faulty rotor conditions. Two speed conditions are presented here. For each steady state result, data was recorded for 10 seconds at 2kHz and analysed offline using the proprietary FFT function in MATLAB.

Figures 1 and 2 show the line current spectra for the two healthy test rigs operating at 1560 and 1590rev/min respectively. The two spectra show comparable harmonic content despite different rotor resistances, interspersed with additional frequencies indicative of the two different operating environments. The Durham test rig spectrum, for example, indicates an increased level of supply unbalance through a greater number of supply time harmonics, notably the even harmonics which are not present in the Manchester supply. Of particular interest are frequencies labelled (a) and (b) for the healthy machines. These frequencies are always present in the machines and result from physical design artefacts such as machine winding layout. Using equation (1) we can calculate these frequencies by setting $k = l = 1$ since

these are fundamental to the machine. Values for these are given in Table 1. The spectra respond as expected from equation (1) and are consistent across both machines. Small variations from the calculated values are a result of minor differences in speed from the demanded value.

WRIG Speed (rev/min)	f_a	f_b
1560	262 Hz	362 Hz
1590	268 Hz	238 Hz

Table 1: Frequencies in line current due to machine layout

Figures 3 and 4 show the line current spectra after rotor unbalance conditions were applied. Firstly, it can be seen that the frequencies (a) and (b) given above remain consistent in the faulty machines as do the supply time harmonics. It is also clear that there is an increase in the harmonic content of the signal from the faulty generators from both test rigs. Frequencies of interest are labelled for each case. Points (c) and (d) are related directly to $-2sf$ components around supply harmonics and these are consistent for both test rigs. However, it should be noted that there is a much greater increase in harmonic content for the Manchester test rig, most notably in points (e) and (f). This is a result of a lower background rotor resistance compared to the Durham test rig and therefore greater speed ripple in the presence of a fault. The observed current frequencies are calculable using equation (2) and are supported by a detailed time-stepped model described in [3].

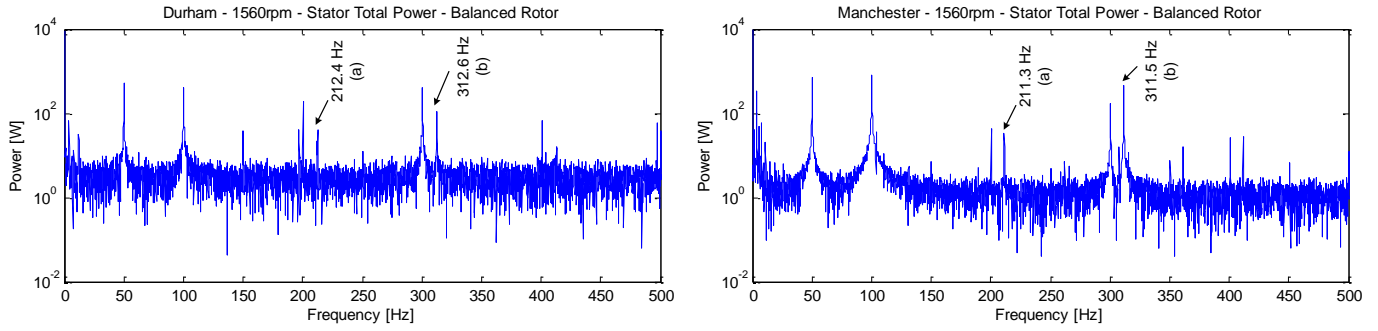


Figure 5: Total instantaneous power spectra for the healthy test rigs at 1560rpm

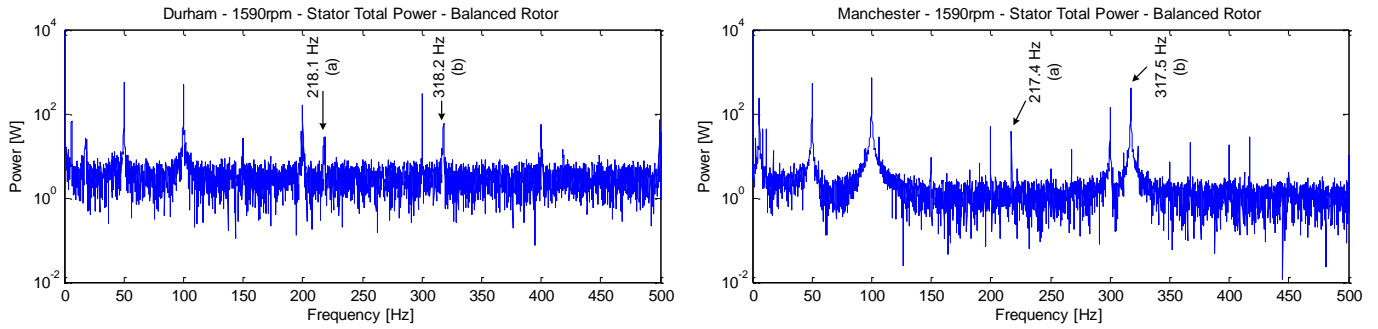


Figure 6: Total instantaneous power spectra for the healthy test rigs at 1590rpm

3.2 Total Instantaneous Power Results

Similar consistency is seen from Figures 5 and 6 for the total instantaneous power spectra at different test rigs and operating speeds, 1560 and 1590 rev/min respectively. Again, frequencies (a) and (b) are visible for both machines with the expected 50Hz shift between current and total instantaneous

power. Equation (3) gives these frequencies as well as those relating to supply unbalance, particularly present in the Durham supply.

Applying the fault we find a similar result to that for current, in that the Manchester results show a greater level of high frequency content. Figures 7 and 8 show the frequencies of interest labelled (c) to (f). Points (c) and (d) are consistent

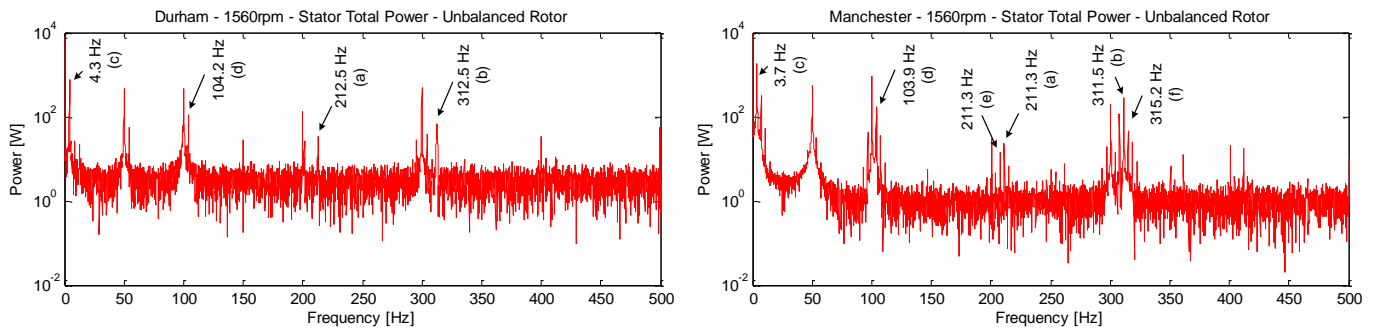


Figure 7: Total instantaneous power spectra for the faulty test rigs at 1560rpm

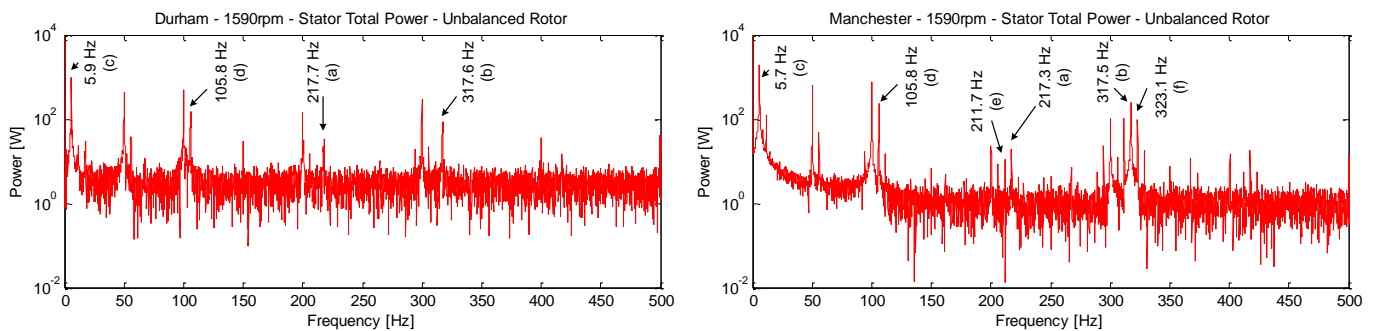


Figure 8: Total instantaneous power spectra for the faulty test rigs at 1590rpm

between the two test rigs and are the direct shift of (c) and (d) in the current spectra. As for current, the higher frequency harmonics (e) and (f) are only visible in the Manchester results. This demonstrates a certain level of dependence upon the machine conditions themselves such that frequencies (a) to (d) show for both machines while other expected components are only visible for the Manchester machine with lower rotor resistance.

3.3 Selection of Constants

For condition monitoring it would be impractical to observe and track all of the frequencies given by equations (1) to (4). As seen in results in the steady state, it would not always be necessary as not all frequencies given by equations (1) to (4) are present in the current or power spectra. As a result of this and to simplify monitoring, a reduced set of frequencies should be defined and constants identified. Values for frequencies (a) to (f) are defined in Table 2 and their respective equations given. It is clear from Table 2 that frequencies (c) to (f) are found by a systematic increase in constant k . While components shown for (e) and (f) are not clear in the Durham test rig data results they have been included in Table 2 as it is expected that these would be clear in a machine with a low rotor resistance as would generally be expected in a WRIG.

Frequency Label	Equation	k	l
50Hz Multiples	$f_{ind}^k = 6k(1-s) \pm l f$	0	1,2,3,..
a, b (Healthy)	$f_{ind}^k = 6k(1-s) \mp l f$	1	1
a, b (Faulty)	$f_{ind}^k = \left \frac{k}{p}(1-s) \mp l \right f$	12	1
c, d	$f_{ind}^k = \left \frac{k}{p}(1-s) \mp l \right f$	4	1
e	$f_{ind}^k = \left \frac{k}{p}(1-s) + l \right f$	8	1
f	$f_{ind}^k = \left \frac{k}{p}(1-s) - l \right f$	16	1

Table 2: Constants for healthy and faulty line current spectra

Constants defining the frequencies found in the total instantaneous power signal are given in Table 3, using equations (3) and (4). It is clear that these are highly consistent with those for line current, which is to be expected.

Frequency Label	Equation	J	k	l
50Hz Multiples	$f_{ind}^k = j \pm 6k(1-s) \pm l f$	1,2, ...	0	1,2 ...
a, b (Healthy)	$f_{ind}^k = j \mp 6k(1-s) \pm l f$	1	1	1

a, b (Faulty)	$f_{ind}^k = \left j \mp \frac{k}{p}(1-s) \pm l \right f$	1	12	1
c, d	$f_{ind}^k = \left j \mp \frac{k}{p}(1-s) \pm l \right f$	1	4	1
e	$f_{ind}^k = \left j - \frac{k}{p}(1-s) + l \right f$	1	8	1
f	$f_{ind}^k = \left j - \frac{k}{p}(1-s) + l \right f$	1	16	1

Table 3: Constants for healthy and faulty total power spectra

4 Results at Variable Speed

Modern WTs > 1 MW generally operate at variable speed, therefore having obtained a set of constants which give consistent results between machines, the Durham test rig was run at variable speed to investigate the potential for fault frequency tracking. The driving conditions were based on a detailed WT model giving similar speed variability to that found in a real wind turbine. Figure 9 shows the result of applying the short term Fourier transform to a 45 second line current data set. A rotor unbalance with the same magnitude as for constant speed was introduced to the WRIG after 15s. The prominent frequencies observed are shown in Figure 9. As expected from constant speed operation, a number of fault frequencies (c, d, e, f) are observed alongside those always present for the machine (a, b) and odd supply harmonics. As expected from equations (1) and (2), both healthy and faulty frequencies shift as the speed of machine varies with time.

Similar consistency is observed for the total instantaneous power signal in Figure 10. Again, frequencies found in both the healthy and faulty machines are present and can be seen to move with the changing WRIG speed.

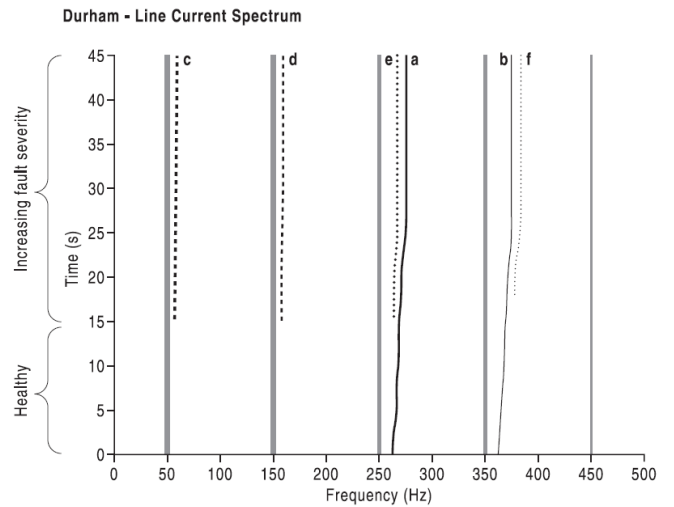


Figure 9: Line current spectrum at variable speed

A proven method for frequency tracking is given in [7] where an accurate speed signal is measured and used to calculate the relevant frequency of interest. Wavelet analysis is carried out to obtain the energy in that frequency for a short time window. The frequency is then recalculated for the next time window to produce a figure showing the changing energy in a fault-dependent, variable frequency.

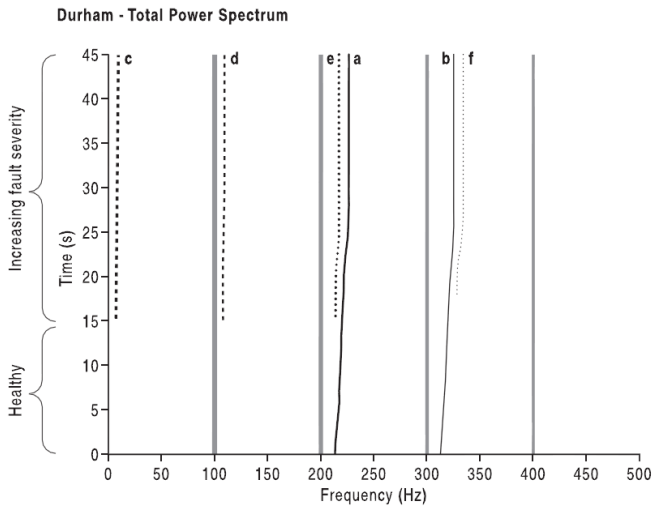


Figure 10: Total power spectrum at variable speed

5 Conclusions

From the work described in this paper we can conclude that:

- Healthy and faulty wound rotor induction machines have clearly defined and calculable frequencies in current and power signals which can be predicted using the analytical expressions given;
- These electrical faults can be detected on two different test rigs in steady state operation;
- The results from the two test rigs are comparable despite variations in operating environment;
- A set of constants can be selected which yield consistent results between different machine test rigs, and;
- Rotor electrical unbalance faults can be detected during variable speed operation, representative of that experienced on a wind turbine, using frequency tracking based on the analytical expressions.

Further work will include deeper investigation of electrical fault frequencies and their detection in different test rig environments. In particular, practical analysis of faulted signals using frequency tracking based on the results of this paper.

Acknowledgements

This work is funded as part of the UK EPSRC Supergen Wind Energy Technologies programme, EP/D034566/1.

References

- [1] Y. Amirat, M. E. H. Benbouzid, B. Bensaker, R. Waumkee, "Generators for Wind Energy Conversion Systems: State of the Art and Coming Attractions", *Journal of Electrical Systems*, Vol. 3-1, pp. 26-38, (2007).
- [2] M. E. H. Benbouzid, "A Review of Induction Motor Signature Analysis as a Medium for Faults Detection", *IEEE Transactions on Industrial Electronics*, Vol. 47, No. 5, (2000).
- [3] S. Djurovic, S. Williamson, A. Renfrew, "Dynamic Model for Doubly-fed Induction Generators with Unbalanced Excitation, both With and Without Faults", *IET Electric Power Applications*, Vol. 3, Iss. 3, pp. 171-177, (2009).
- [4] W. Q. Jeffries, J. A. Chambers, D. G. Infield, "Experience with Bicoherence of Electrical Power for Condition Monitoring of Wind Turbine Blades", *IEE Proc. Vision, Image and Signal Processing*, Vol. 145, No. 3, pp. 141-148, (1998).
- [5] S. F. Legowski, A. H. M. Sadrul Ula, A. M. Trzynadlowski, "Instantaneous Power as a Medium for the Signature Analysis of Induction Motors", *IEEE Transactions on Industrial Applications*, Vol. 32, No. 4, (1996).
- [6] S. Williamson, S. Djurovic, "Origins of Stator Current Spectra in DFIGs with Winding Faults and Excitation Asymmetries", *Proc. Of IEEE IEMDC 2009 Miami*, pp.563-570, (2009).
- [7] W. Yang, P. J. Tavner, C. J. Crabtree, M. Wilkinson, "Cost-Effective Condition Monitoring for Wind Turbines", *IEEE Transactions on Industrial Electronics*, Vol. 57, No. 1, pp. 263-271 (2010).